2024 International Conference on Simulation of Semiconductor Processes and Devices (SISPAD) | 979-8-3315-1635-2/24/$31.00 ©2024 IEEE | DOI: 10.1109/SISPAD62626.2024.10733341

First-principles study of the origins of random telegraph noise in MoS_2/hBN-based field-effect transistors

Ryong-Gyu Lee
The School of Electrical Engineering
Korea Advanced Institute of Science and Technology (KAIST)
Yuseong-gu, Daejeon, Korea
ronggyulee@kaist.ac.kr

Jiyoon Song
The School of Electrical Engineering
Korea Advanced Institute of Science and Technology (KAIST)
Yuseong-gu, Daejeon, Korea
jiyoon.song@kaist.ac.kr

Yong-Hoon Kim
The School of Electrical Engineering
Korea Advanced Institute of Science and Technology (KAIST)
Yuseong-gu, Daejeon, Korea
y.h.kim@kaist.ac.kr

***Abstract*—In the development of nanoscale field-effect transistor (FET) devices, defects in the gate dielectric are becoming a more critical factor for device reliability. However, the atomistic understanding of the instabilities in threshold voltage such as bias-temperature instabilities, 1/f noise, and random telegraph noise (RTN) remains limited. Herein, we describe our effort in establishing first-principles theoretical tools for the analysis of RTN. We consider hexagonal boron nitride (hBN)-encapsulated MoS_2-based 2D FETs, with various defect candidates introduced in the hBN layer. Based on the multi-space constrained-search density functional theory framework, we study the defect energetics under different temperature and gate-bias conditions. Mapping to the non-radiative multi-phonon model, configuration coordinate diagram analyses provide the classical activation barriers for defect trapping/de-trapping behaviors and capture and emission times for RTN. Our results reveal that both hBN C_B and V_N defects can contribute to fast and slow RTNs for the MoS_2 FET, respectively.**

Keywords—field-effect transistor, defect, random telegraph noise (RTN), non-equilibrium first principles calculation

I. Introduction

Recently, Si-based field effect transistor (FET) has entered the sub-10-nm technology nodes, however continued scaling is increasingly challenging because the gate electrostatics for the three-terminal device require substantial reduction in channel thickness to preserve desired gate-controllability. While tremendous efforts have been made to reduce the channel thickness, achieving this for three-dimensional (3D) semiconductor devices is challenging due to unavoidable finite thickness variation, surface roughness and dangling bonds, which increase scattering of carriers and thus result in mobility degradation. To overcome this challenge, two-dimensional (2D) semiconductors, such as transition metal dichalcogenides (TMDs) have been emerged as promising channel materials for FETs. However, in realizing 2D FETs, defects in the gate dielectric can be critical barrier to device reliability, leading to instabilities in threshold voltage, such as bias-temperature instabilities, flicker (1/f) noise, and random telegraph noise (RTN). Specifically, the border traps in gate insulator can capture or emit the carriers, causing the hysteresis of the gate transfer characteristics. Although these instability problems have been intensively studied for the conventional Si-based devices [1], a comprehensive understanding of threshold voltage instabilities for 2D FET is still limited.

In this study, we investigate atomistic origin of RTN in hexagonal boron nitrides (hBN) encapsulated-MoS_2 based 2D FETs by adopting Au/4-layer (4L) hBN/MoS_2 heterostructure models [Fig. 1a]. As potential candidates of RTN, we consider carbon (C) and oxygen (O) impurities (C_N, C_B, and O_N), and native nitrogen vacancy (V_N) at hBN layer [Fig. 1b], which are experimentally or theoretically reported as dominant defects in hBN [2]. Introducing these defects into the second hBN layer near MoS_2, we evaluate their equilibrium electronic structures and confirm that the C_N defect potentially acts as acceptor-type defect and the C_B, V_N, and O_N defects can act as donor-type defect for MoS_2 channel. We next examine defect dynamics for the different temperature and gate-bias conditions, in which the self-consistent electron filling at defect influences their energy level movements. Finally, based on the configuration coordinate diagram analyses, we calculate activation barriers for the trapping/de-trapping of the defects and evaluate their capture and emission times for RTN. Further analysis proves that both C_B, V_N can contribute to fast and slow RTN, respectively.

II. Method

DFT and MS-DFT calculations: In modeling the hBN encapsulated-MoS_2 based 2D FETs, we adopted single-layer Au/ vacuum/four-layer hBN/single-layer MoS_2 heterostructure and introduced the C_N, C_B, V_N, and O_N into the second interfacial hBN layer. The simulation cell contained 5×5 supercell of hBN, 4×4 supercell of MoS_2, and 5x5 supercell of Au(111) to minimize the lattice mismatch. To obtain equilibrium electronic structures, we performed density functional theory (DFT) calculations using the SIESTA software package [3] within the LDA exchange-correlation functional [4]. The atomic cores were replaced by norm-conserving pseudopotentials of Troullier-Martins type [5], and the double ζ-plus-polarization-level numerical atomic orbital basis sets were employed. For nonequilibrium calculations, we used multi-space constrained search DFT (MS-DFT) [6-8] that enables us to apply gate bias (V_g) between MoS_2 channel and Au double electrodes. To obtain the configuration coordinate diagram, we performed MS-DFT

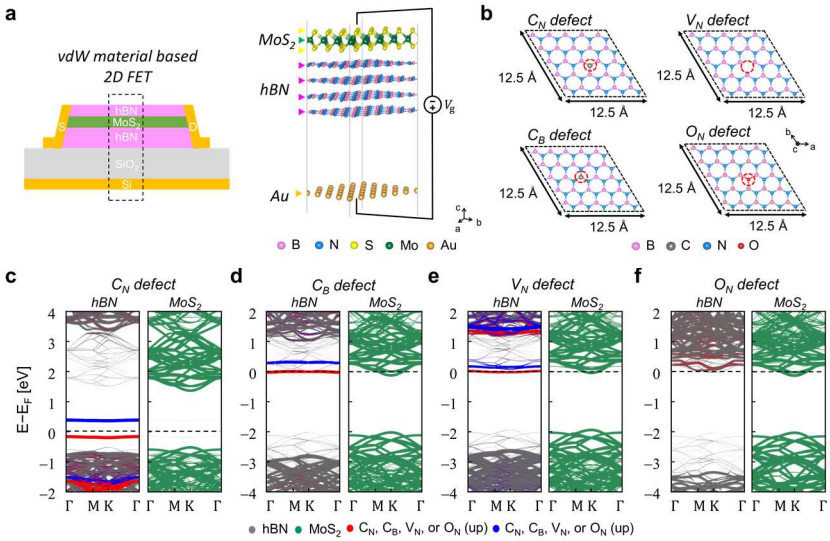

Fig. 1. (a) The schematics of MoS_2 based 2D FET (left) and employed calculation model of Au/4L hBN/MoS_2 structure (right). (b) As potential candidates of RTN, the C_N, C_B, V_N, and O_N defects in hBN layer. The equilibrium band structures of (c) C_N, (d) C_B, (e) V_N, and (f) O_N defects.

calculations for a simple Au/monolayer hBN model introducing a defect within the hBN layer and calculated the total energy by varying the charged states of the defect.

III. Results and Discussion

We first provide equilibrium band structures of C_N, C_B, V_N, and O_N defects at hBN layer in Au/4L hBN/MoS_2 [Fig. 1c-f]. It shows that the C_N forms defect states near the valence band maximum (VBM) of MoS_2 that can act as acceptor-type defect, whereas the C_B, V_N, and O_N form defect states near the conduction band minimum (CBM) of MoS_2 that potentially act as donor-type defects for MoS_2 channel. However, the O_N defect exhibits shallow states within the CBM of hBN, making it hardly to contribute to RTN as a broader trap. In addition, given that the RTN is caused by charge transfer between the defect within the dielectric and the channel, the C_N defect is energetically far from the valence band of MoS_2 (0.3 eV above the VBM), making it more difficult to contribute to RTN compared to other defects located within the conduction band of hBN.

Having confirmed that the donor-type C_B and V_N are potential candidates for RTN, we further analyzed their defect energy levels and occupations under different temperatures and gate bias conditions, which significantly attribute to the RTN characteristics. Applying the V_g to Au/4L hBN/MoS_2, we estimated the V_g- and T-dependent energetic positions of the defect level E_T and the corresponding occupations for both C_B and V_N cases [Fig. 2]. For the C_B case, at V_g = −18.5 V, the unoccupied defect state locates above the Fermi level (E_F) of MoS_2 channel for all temperature cases [Fig. 2a and 2c]. As the V_g increases, the C_B state rapidly moves closer to the E_F and then slowly downshifts near the E_F. This is due to the electron filling of unoccupied C_B state which increases its energy to align with the E_F. It should be also noted that for higher temperature case (T = 250 K), the C_B state reaches to the E_F at a higher V_g = −10.5 V compared to the lower temperature case (T = 50 K). It can be seen that the extended Fermi-Dirac distribution tail making the states hardly shift below the E_F by the electron filling. In addition to detailed analyses of the C_B defect dynamics under different V_g and temperatures, we also explored the V_N case and found that it shows almost identical behavior to the C_B case [Fig. 2b and 2d].

While both C_B and V_N show similar defect energy level dynamics with respect to V_g the and temperature, they can be further characterized by examining the capture (τ_c) or emission time constant (τ_e) in RTN, associated with the charge transfer between defect and the channel. Conventionally, the nonradiative multi-phonon (NMP) model [9], employing the configuration coordinate diagram which replaces vibrational modes with a single effective phonon mode, is utilized to evaluate the NMP charge transfer rates. Within the configuration coordinate diagram, the total energies for neutral or charged defect state is described as a function of configuration coordinate Q, which quantifies the one-dimensional effective phonon mode. To analyze the capture (trapping) and emission (de-trapping) processes in RTN, the total energy surface of

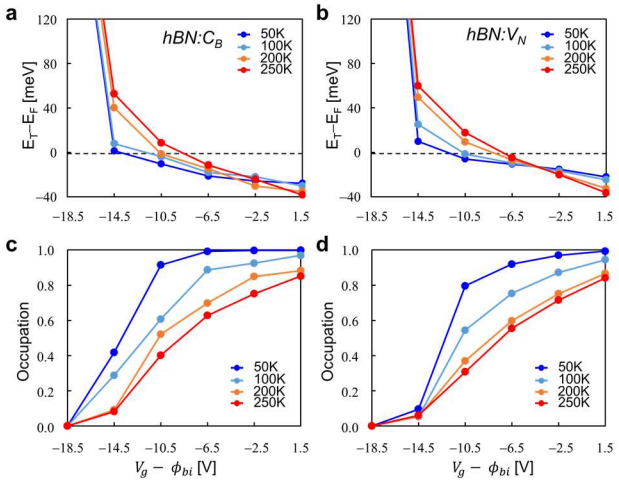

Fig. 2. The energetic positions of the defect level E_T of (a) C_B and (b) V_N for T = 50, 100, 200 and 250 K. The corresponding occupation of (c) C_B and (d) V_N for T = 50, 100, 200 and 250 K.

capture or emission state is approximated by parabola curves as follow [10],

$$E_{\{c,e\}}(Q) = \frac{1}{2} M_{\{c,e\}} \Omega^2_{\{c,e\}} (Q - Q^0_{\{c,e\}}) + E^0_{\{c,e\}} \quad (1)$$

, where the $M_{\{c,e\}}$ and $\Omega_{\{c,e\}}$ modal mass and frequency of effective vibration for the capture or emission state, respectively. The $Q^0_{\{c,e\}}$ and $E^0_{\{c,e\}}$ are position and height of the parabola curve for the capture or emission state, respectively. Using the configuration coordinate diagram, the defect deformation can measured by estimating the total mass weighted distortion ΔQ. The Huang-Rhys factor $S_{\{c,e\}}$ is defined as follow,

$$S_{\{c,e\}} = \frac{1}{2\hbar} \Delta Q^2 \Omega_{\{c,e\}} \quad (2)$$

We note that the $E^0_{\{c,e\}}$ depends on the external V_g, which moves the defect level E_T. Therefore, we assumed $E_T - E_F = E^0_c - E^0_c$.

We then evaluated the configuration coordinate diagram for the C_B and V_N in the monolayer hBN [Fig. 3a]. The calculated ΔQ are 0.25 and 0.71 amu$^{1/2}$Å for C_B and V_N, respectively, and the corresponding Huang-Rhys factor S_e are 1.2 and 4.5, for C_B and V_N, respectively, indicating a stronger electron–phonon coupling for the V_N case. We also obtained the capture (E^a_c) and emission activation energies (E^a_e) by identifying the intersection between the capture and emission total energy curves. According to the NMP model, in the high temperature (classical) limit where the thermal activation dominates the charge transfer, the τ_c or τ_e for RTN are determined by the classical E^a_c or E^a_e as follow,

$$\tau_{\{c,e\}} = \tau_0 \exp\left(\frac{E^a_{\{c,e\}}}{kT}\right) \quad (3)$$

, where the $1/\tau_0$ is proportional to the capture cross section. In Fig. 3b, we provide the calculated the τ_c and τ_e for C_B and V_N as a function of V_g for T = 250 K. For both cases, we found that as the V_g increases, τ_e increases and τ_c decreases, indicating that the defect more readily traps the electrons which is also consistent with the increased defect occupation [Fig. 2c and 2d]. On the other hand, the C_B shows smaller τ_e and τ_c compared to the V_N. This is attributed to the smaller lattice relaxation (ΔQ = 0.25 amu$^{1/2}$Å) and electron-phonon coupling in C_B (S_e= 1.18), leading to smaller activation energies compared to those of V_N with larger lattice relaxation (ΔQ = 0.71 amu$^{1/2}$Å) and electron-phonon coupling (S_e= 4.49). Our result shows that, in the high temperature limit, the C_B and V_N can contribute to fast and slow RTN, respectively. We comment that while our study focuses on the high-temperature limit where thermal activation pronounces the charge transfer mechanism by evaluating the activation energies, to elucidate the NMP transition rates for the lower temperature limit, in which the quantum tunneling between barriers significantly affects charge transfer, the quantum mechanical formalism should be employed in the calculation [9].

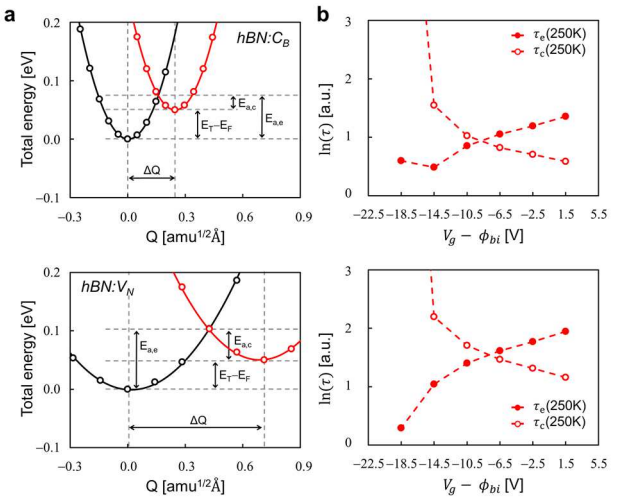

Fig. 3. (a) Calculated configuration coordinate diagram for the C_B (top panel) and V_N (bottom panel), indicating the potential energy surfaces for capture (black curve) and emission (red curve) states. The E^a_c and E^a_e are the capture and emission activation energies, respectively. (b) Calculated τ_e (filled circle) and τ_e (unfilled circle) for the C_B (top panel) and V_N (bottom panel) a function of V_g at 250 K.

IV. Conclusion

To summarize, performing DFT and MS-DFT calculations, we explored the atomistic mechanism of RTN in the MoS_2 based 2D FETs by adopting Au/hBN/MoS_2 heterostructure models. To identify potential candidates of RTN, we introduced the C_N, C_B, O_N, and V_N at second hBN layer, and obtained their defect levels, revealing that the donor-type C_B and V_N are potentially contribute to the RTN. Demonstrating the defect energy level dynamics of C_B and V_N under different temperatures and gate-biases, we found that the C_B and V_N shows energetically similar behavior. Employing the NMP model with the configuration coordinate diagram analyses, we evaluated the τ_c and τ_e for RTN and identified that the C_B and V_N can contribute to fast and slow RTN in the thermal activation limit, respectively. Our study provides theoretical tool for understanding of RTN, which is crucial for improving the performance and reliability of next-generation 2D FETs.

Acknowledgment

This work was supported by the National Research Foundation of Korea (2023R1A2C2003816, RS-2023-00253716).

References

[1] Y. Xue *et al.*, "On the Understanding of pMOS NBTI Degradation in Advance Nodes: Characterization, Modeling, and Exploration on the Physical Origin of Defects," *IEEE Trans. Electron Devices,* vol. 70, no. 9, pp. 4518-4524, 2023

[2] L. Weston, D. Wickramaratne, M. Mackoit, A. Alkauskas, and C. G. Van de Walle, "Native point defects and impurities in hexagonal boron nitride," *Phys. Rev. B,* vol. 97, no. 21, p. 214104, 2018

[3] J. M. Soler *et al.*, "The SIESTA method for *ab initio* order-*N* materials simulation," *J. Phys. Condens.,* vol. 14, no. 11, pp. 2745-2779, 2002

[4] D. M. Ceperley and B. J. Alder, "Ground State of the Electron Gas by a Stochastic Method," *Phys. Rev. Lett.,* vol. 45, no. 7, pp. 566-569, 1980

[5] N. Troullier and J. L. Martins, "Efficient pseudopotentials for plane-wave calculations," *Phys. Rev. B,* vol. 43, no. 3, pp. 1993-2006, 1991
[6] J. Lee, H. S. Kim, and Y. H. Kim, "Multi-Space Excitation as an Alternative to the Landauer Picture for Nonequilibrium Quantum Transport," *Adv. Sci.,* vol. 7, no. 16, p. 2001038, 2020
[7] J. Lee, H. Yeo, and Y. H. Kim, "Quasi-Fermi level splitting in nanoscale junctions from ab initio," *PNAS,* vol. 117, no. 19, pp. 10142-10148, 2020
[8] T. H. Kim, J. Lee, R.-G. Lee, and Y.-H. Kim, "Gate- versus defect-induced voltage drop and negative differential resistance in vertical graphene heterostructures," *Npj Comput. Mater.,* vol. 8, no. 1, 2022
[9] T. Grasser, "Stochastic charge trapping in oxides: From random telegraph noise to bias temperature instabilities," *Microelectron. Reliab.,* vol. 52, no. 1, pp. 39-70, 2012
[10] A. Alkauskas, Q. Yan, and C. G. Van de Walle, "First-principles theory of nonradiative carrier capture via multiphonon emission," *Phys. Rev. B,* vol. 90, no. 7, p. 075202, 2014